

First-principle studies of spin-electric coupling in a $\{Cu_3\}$ single molecular magnet

M. Fhokrul Islam, Javier F. Nossa, and Carlo M. Canali

School of Computer Science, Physics and Mathematics, Linnaeus University, Kalmar-Sweden

Mark Pederson

Naval Research Laboratory, Washington, USA

(Dated: November 11, 2018)

We report on a study of the electronic and magnetic properties of the triangular antiferromagnetic $\{Cu_3\}$ single-molecule magnet, based on spin density functional theory. Our calculations show that the low-energy magnetic properties are correctly described by an effective three-site spin $s = 1/2$ Heisenberg model, with an antiferromagnetic exchange coupling $J \approx 5$ meV. The ground state manifold of the model is composed of two degenerate spin $S = 1/2$ doublets of opposite chirality. Due to lack of inversion symmetry in the molecule these two states are coupled by an external electric field, even when spin-orbit interaction is absent. The spin-electric coupling can be viewed as originating from a modified exchange constant δJ induced by the electric field. We find that the calculated transition rate between the chiral states yields an effective electric dipole moment $d = 3.38 \times 10^{-33} \text{ C m} \approx e10^{-4} a$, where a is the Cu separation. For external electric fields $\varepsilon \approx 10^8$ V/m this value corresponds to a Rabi time $\tau \approx 1$ ns and to a δJ of the order of a few μeV .

I. INTRODUCTION

Single-molecule magnets (SMMs) have been intensively studied in the last two decades (for a review see Ref. 1). At low temperature these remarkable molecules behave in part like bulk magnets thanks to their very long magnetization relaxation time. At the same time SMMs are genuine quantum systems. They display a variety of non-trivial quantum effects such as the quantum tunneling of the magnetization,^{2,3} Berry phase interference,⁴ and quantum spin coherence⁵. Due to their double nature, SMMs are ideal systems to investigate decoherence and the interplay between classical and quantum behavior.⁵

From the point of view of applications, interest in SMMs has been in part spurred by the possibility that these structures could represent the ultimate molecular-scale limit for magnetic units in high-density magnetic storage materials. More recently SMMs have been recognized as promising building blocks in molecular spintronics, the emerging field combining spintronics and molecular electronics.⁶⁻¹¹ In particular, thanks to their long spin coherence time,⁵ SMMs are good candidates to realize spintronic devices that maintain, control and exploit quantum coherence of individual spin states. These devices could find important applications in the field of quantum information processing.^{12,13}

One key issue in using SMMs in molecular spintronics and quantum information processing is the ability of switching efficiently between their different magnetic states. The conventional way of manipulating magnetic states is by applying an external magnetic field. However, this approach has signif-

icant drawbacks when it comes to controlling magnetic states at the molecular level. Quantum manipulation of SMM requires application of an external field at a very small spatial and temporal scale. It is, however, very difficult to achieve such a small scale manipulation using standard electron- spin control techniques such as electron spin resonance (ESR) driven by ac magnetic field.⁵

One promising alternative to achieve control of magnetic states at the molecular level is to use an electric field instead. Typically, by using STM tips for example, it is possible to apply strong time-dependent electric fields in sub-nano regions, with time scales of 1 ns.^{14,15} Clearly, since electric fields do not couple directly to spins, it is essential to find efficient mechanisms for spin-electric coupling as well as real SMMs where this mechanism can be at play. In principle an electric field can interact with spins indirectly via the spin-orbit interaction. However, since the strength of the coupling scales like the volume of the system, this mechanism is not the most efficient one for manipulating SMMs.

Recently, it has been proposed¹⁶ that in some molecular antiferromagnets lacking inversion symmetry, such as the triangular antiferromagnetic $\{Cu_3\}$ and other odd-spin rings, an electric field can efficiently couple spin states through a combination of exchange and chirality of the spin-manifold ground state¹⁶. The $\{Cu_3\}$ molecule, while large^{17,18}, reduces to a simple model composed of three identical spin $s = 1/2$ Cu cations coupled by an antiferromagnetic (Heisenberg) exchange interaction. Its ground state consists of two total-spin $S = 1/2$ doublets of opposite spin chirality, degenerate in the absence of spin-orbit interaction. Accord-

ing to an analysis based on group theory,^{16,19} due to the lack of inversion symmetry, an electric field can couple states of opposite chirality through the dipole operator, even when spin-orbit interaction is absent. In the presence of an additional small dc magnetic field that mixes the spin states, this spin-electric coupling will then generate efficient electric transitions from one spin state to another.

An intuitive picture of this coupling is the following. Since a spin $S = 1/2$ triangular antiferromagnet is frustrated, there exist three energetically degenerate antiferromagnetic spin configurations for $S_z = 1/2$ and three for $S_z = -1/2$. Both ground state chiral eigenstates, with a given value of S_z , are appropriate, equally weighted, linear combinations of these three frustrated spin configurations. Each of these three configurations, if prepared, would have a dipole moment with the same magnitude that points from the antiparallel sites to the midpoint between the two parallel sites. While the net dipole moment of the two chiral eigenstates is zero, the dipole transition matrix element between them is not and it is simply related to the magnitude of the permanent dipole moment of the energetically degenerate frustrated configurations.

In practice the relevance of this spin-electric mechanism depends on the coupling strength of the chiral states by the electric field, *i.e.* on the value of the dipole moment of the frustrated spin configurations. Theoretically this is an issue that only a microscopic calculation for the specific molecule can address. The main objective of this work is to calculate the strength of this coupling for the $\{Cu_3\}$ molecule using *ab-initio* methods. Our approach is based on Spin Density Functional Theory (SDFT), implemented in the NRLMOL codes, which has been very successful in describing the electronics and magnetic properties of Mn_{12} -acetate and other SMMs.²⁰⁻²³ Recently SDFT implemented in NRLMOL has been used in a first-principle study of quantum transport in a Mn_{12} single-electron transistor.²⁴

Our results show that indeed the crucial electric-dipole moment is not negligible in $\{Cu_3\}$ and it would correspond to characteristic Rabi times of 1 ns in the presence of typical electric fields generated by STM tips. As originally suggested in Ref. 16, the spin-electric coupling can be interpreted as due to a modified exchange interaction brought about by the electric field. Although here we only address the specific case of $\{Cu_3\}$, our paper introduces a methodology that can be followed in a systematic study of other SMMs without inversion symmetry.

The paper is organized as follows. In section II we discuss the electronic and magnetic properties of triangular $\{Cu_3\}$ molecule based on *ab-initio* calculations and show that the low-energy quantum prop-

erties of the molecule can be described by an effective three-spin $s = 1/2$ Heisenberg model with antiferromagnetic coupling. In section IIB we review the underlying mechanism of spin-electric coupling in $\{Cu_3\}$ antiferromagnet, based on the effective spin Hamiltonian. The first-principle computation of the spin-electric coupling and electric dipole moment of $\{Cu_3\}$ is presented in section IV. In section IVB we discuss the effect of the electric field on the exchange coupling. Finally we present the summary of our work in section V.

II. ELECTRONIC AND MAGNETIC PROPERTIES OF $\{Cu_3\}$

A. Microscopic description of the molecule

The $\{Cu_3\}$ molecule that we are interested in has chemical composition $Na_{12}[Cu_3(AsW_9O_{33})_2 \cdot 3H_2O] \cdot 32H_2O$ ¹⁷. This molecule has been studied experimentally by different groups.^{17,18} The three Cu^{2+} cations form an equilateral triangle and, as we show below, are the sites of three identical $s = 1/2$ quantum spins. The frontier electrons on each of these sites have primarily d character. The bridging atoms consist of predominantly paired electrons and are only polarized to the degree that the same-spin states hybridize with the unpaired d -electrons on the Cu sites. Due to the localized nature of transition-metal 3d states, direct exchange stabilization due to parallel neighboring states is expected to be exponentially small. Therefore, unless the frontier d -electrons are spatially orthogonal by symmetry to the d -electrons on other sites, *antiferromagnetic ordering* between electrons on a pair of neighboring Cu atoms is energetically preferred due to the increase in the system's kinetic energy, induced by orthogonality constraints, when neighboring states are parallel.

Although the spin model of three exchange-coupled spin $1/2$ is quite useful to understand the magnetic properties of the $\{Cu_3\}$ SMM, all the other atoms in the molecule are essential for its geometrical stability and for the resulting superexchange interaction among the spins at the Cu sites. A proper *ab-initio* description of the molecule must therefore include to a certain extent all these atoms.

Building a suitable model of the molecule is a considerable challenge since the model molecule should preserve the essential physics. We have constructed the molecule by preserving the D_{3h} symmetry of the polyanionic part of the molecule as observed in the experiment.^{17,18} Three of the twelve Na atoms of the molecule are placed at the belt region of the molecule. These three are the most important of all

the Na atoms for the stability of the belt region of the molecule. There is some uncertainty in the position of the Na atoms but we have placed eight of the remaining nine Na atoms in a way to preserve the D_{3h} symmetry. The last Na atom is replaced by a H atom and is placed at the center of the molecule to maintain the charge neutrality of the valance electrons. The model of the molecule used in this calculation is shown in Fig. 1.

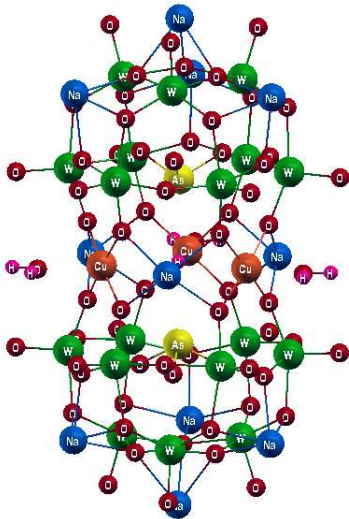


FIG. 1: Model of the $\{Cu_3\}$ molecule with chemical composition $Na_{11}H[Cu_3(AsW_9O_{33})_2 \cdot 3H_2O]$ used in this work. Xcrystden visualization tool²⁵ is used for this figure.

We have relaxed the geometry using the *ab-initio* package NRLMOL^{26,27} that uses a Gaussian basis set to solve the Kohn-Sham equations using PBE-GGA approximation.²⁸ All-electron calculations are performed for all elements of the molecule except for tungsten, for which we have used pseudo potentials. The relaxation is first performed by setting the net total spin of the molecule to $S = 3/2$ and then by changing the net spin to $1/2$. Self-consistency is reached when the total energy is converged to 10^{-6} Hartree or less.

The density of states of the molecule is shown in Fig. 2. The HOMO-LUMO gap for the majority spin is calculated to be about 0.78 eV and that for minority spin is about 0.58 eV. Although in our calculations we have used an equilateral arrangement of the three Cu atoms, it is found experimentally that the $\{Cu_3\}$ molecule in the ground state is slightly distorted into an isosceles triangle.¹⁷ Since the calculated HOMO-LUMO gap for the equilateral configuration is relatively large, the distortion is likely to be due to magnetic exchange rather than to the Jahn-Teller effect.

One important result of our calculations, after the

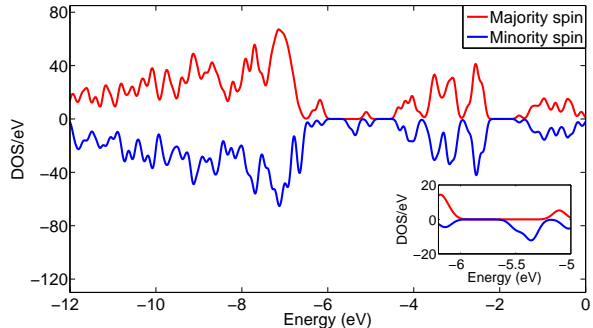


FIG. 2: Density of states of $\{Cu_3\}$ molecule. HOMO-LUMO gaps for majority and minority spins are shown in the inset.

geometry relaxation have been implemented, is that the ground state of the system is anti-ferromagnetic, with a net total spin of $1/2$ in accordance with experiment.²⁹ The ground state energy is lower by about 5.6 meV relative to spin $S = 3/2$ configuration. This allows us to assign an exchange constant $J \approx 5$ meV to the three-site Heisenberg spin model mentioned above (see also next Section).

The calculated magnetization density of the relaxed molecule shows the presence of three electron-spin magnetic moments $\mu_i \approx 0.55\mu_B$, $i = 1, 2, 3$, essentially localized at the three Cu atom sites. Note that the orbital moments are quenched. These results confirm that the low-energy properties of the $\{Cu_3\}$ molecule can be approximately described by an effective spin Hamiltonian of three spins $s = 1/2$ localized at the Cu sites.

The exchange coupling between two Cu atoms is indirect and follows a superexchange path¹⁸ along Cu-O-W-O-W-O-Cu as shown in Fig. 3 - see the yellow line connecting the atoms. To understand this coupling mechanism we focus on one of the three CuO_5 complexes of the molecule (shown inside the circle in Fig. 3). Because of the square-pyramidal C_{4v} point-group symmetry of this complex, the d_{xy} , d_{xz} , d_{yz} states of Cu have lower energies compared to the $d_{x^2-y^2}$ and d_{z^2} states. Moreover, our calculation shows that the axial Cu-O distance (2.35 Å) in each unit is larger than the four equatorial Cu-O distances (1.93 Å). Thus the energy of d_{z^2} state is lower than $d_{x^2-y^2}$ state and the unpaired d electron of the Cu^{2+} ion resides in $d_{x^2-y^2}$ state that is directed along the equatorial Cu-O vectors. Therefore, the exchange coupling between two Cu atoms involves three O atoms and two W atoms.

The magnetic moment calculations of the atoms of $\{Cu_3\}$ molecule also support the superexchange path. The magnetic moments at the O and W atoms on this path is much smaller than at the Cu sites,

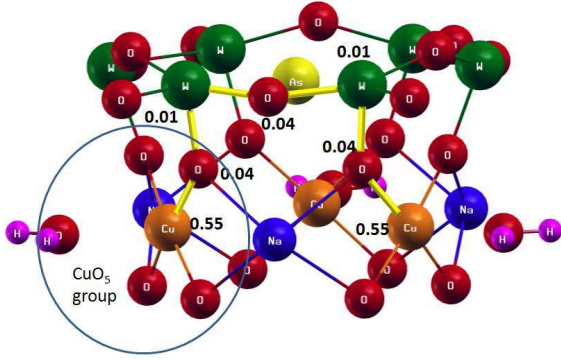


FIG. 3: (Color online) Superexchange coupling between two Cu atoms. The yellow line connecting two Cu atoms through three O and two W atoms shows the path along which spin coupling between Cu atoms is mediated. The numbers near the atoms are the magnetic moment (in units of μ_B) of the atoms along the exchange path.

but still 2 order of magnitude larger than at atoms not belonging to this path.

B. Effective spin Hamiltonian description

Based on the results of the *ab-initio* calculations, the low-energy properties of the $\{Cu_3\}$ molecule can be described by the following quantum spin Hamiltonian

$$H_0 = \sum_{i=1}^3 J_{i,i+1} \mathbf{s}_i \cdot \mathbf{s}_{i+1} + \sum_{i=1}^3 \mathbf{D}_{i,i+1} \cdot \mathbf{s}_i \times \mathbf{s}_{i+1}, \quad (1)$$

where J is the exchange parameter, \mathbf{D} is the Dzyaloshinski vector and \mathbf{s}_i are three spins-1/2, located at the Cu sites. The first term in the Hamiltonian is an isotropic Heisenberg model. The geometry-relaxation and electronic-structure calculations showed that the Cu atoms form an equilateral triangle with a very small intrinsic deformation. Since the atomic environment around each of the the three Cu-Cu bonds is the same, we take the three exchange constants $J_{i,i+1}$ to be the same value, J . On the basis of the splitting between the ferromagnetic and antiferromagnetic configurations discussed in the previous section, J is positive and $\simeq 5$ meV. The second term in Eq. (1) is the anisotropic Dzyaloshinski-Moriya exchange interaction originating from spin-orbit interaction. Its strength $|\mathbf{D}_{i,i+1}|$ is at least one-order of magnitude smaller than the isotropic exchange constant J , and we will disregard it for the moment.

The ground state of Eq. (1) is total spin $S = 1/2$ manifold, which can be constructed in terms of six degenerate spin configurations, three associated with

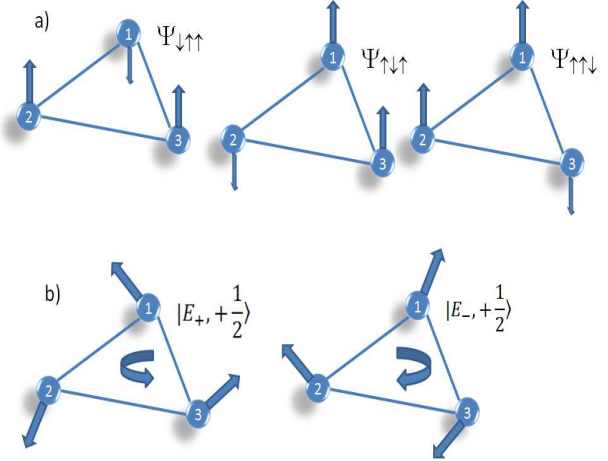


FIG. 4: a) The three spin configurations of the molecule associated with total spin projection $S_z = +1/2$. b) The two chiral states formed from a) with chirality +1 and -1, respectively.

$S_z = +1/2$ and the other three associated with $S_z = -1/2$. Fig. 4 shows the three possible spin configurations associated with $S_z = +1/2$.

The total-spin $S = 3/2$ four-dimensional subspace has an energy of order J above the ground-state manifold.

Within the $S = 1/2$ ground-state manifold, we can construct two degenerate, linearly independent doublets. Specifically the two $S_z = +1/2$ states (shown in Fig. 4(b)) are

$$\begin{aligned} |E_+, +\frac{1}{2}\rangle &= \frac{1}{\sqrt{3}}[\Psi_{\downarrow\uparrow\uparrow} + \omega\Psi_{\uparrow\downarrow\uparrow} + \omega^2\Psi_{\uparrow\uparrow\downarrow}], \\ |E_-, +\frac{1}{2}\rangle &= \frac{1}{\sqrt{3}}[\Psi_{\downarrow\uparrow\uparrow} + \omega^2\Psi_{\uparrow\downarrow\uparrow} + \omega\Psi_{\uparrow\uparrow\downarrow}], \end{aligned} \quad (2)$$

while the $S_z = -1/2$ states are

$$\begin{aligned} |E_+, -\frac{1}{2}\rangle &= \frac{1}{\sqrt{3}}[\Psi_{\uparrow\downarrow\downarrow} + \omega\Psi_{\downarrow\uparrow\downarrow} + \omega^2\Psi_{\downarrow\downarrow\uparrow}], \\ |E_-, -\frac{1}{2}\rangle &= \frac{1}{\sqrt{3}}[\Psi_{\uparrow\downarrow\downarrow} + \omega^2\Psi_{\downarrow\uparrow\downarrow} + \omega\Psi_{\downarrow\downarrow\uparrow}], \end{aligned} \quad (3)$$

where $\omega = e^{i\frac{2\pi}{3}}$. The quantum numbers E_+ and E_- specify the so called handedness or chirality of the states $|E_{\pm}, M\rangle$, which are eigenstates of the chirality operator

$$C_z = \frac{4}{\sqrt{3}} \mathbf{s}_1 \cdot \mathbf{s}_2 \times \mathbf{s}_3, \quad (4)$$

with eigenvalues ± 1 respectively. It is useful to introduce also the other two components of the chiral vector operator

$$C_x = -\frac{2}{3}(\mathbf{s}_1 \cdot \mathbf{s}_2 - 2\mathbf{s}_2 \cdot \mathbf{s}_3 + \mathbf{s}_3 \cdot \mathbf{s}_1), \quad (5)$$

$$C_y = \frac{2}{\sqrt{3}}(\mathbf{s}_1 \cdot \mathbf{s}_2 - \mathbf{s}_3 \cdot \mathbf{s}_1), \quad (6)$$

and the ladder operators $C_{\pm} \equiv C_x \pm iC_y$. Note that $[C_l, C_m] = i2\epsilon_{lmn}C_n$ and $[C_l, S_m] = 0$. Here ϵ_{lmn} is the Levi-Civita symbol. The ladder operators reverse the chirality of the states: $C_{\pm}|E_{\mp}, M\rangle = |E_{\pm}, M\rangle$. Thus \mathbf{C} behaves exactly like the operator \mathbf{S} (for $S = 1/2$) in chiral space.

In the microscopic description of the molecule implemented within density functional theory via the NRLMOL code, the chiral states defined in Eqs. (2) and (3) have to be understood as being composed both of a spin and an orbital part.

We conclude this section with an observation of the DM interaction. As shown in Ref. 16, the DM interaction within the $S = 1/2$ ground state manifold takes the simple form $H_{\text{DM}} = \Delta_{\text{SO}}C_zS_z$, where Δ_{SO} is the effective spin orbit coupling constant. Thus equal-spin states of opposite chirality are split by $2\Delta_{\text{SO}}$.

III. SPIN-ELECTRIC EFFECT IN $\{Cu_3\}$

A. Absence of inversion symmetry and coupling of ground-state chiral states

The triangular spin-1/2 antiferromagnet $\{Cu_3\}$ belongs to the class of antiferromagnetic rings with an odd number of half-integer spins. In these systems, the lack of inversion symmetry of the molecule as a whole implies that the ground-state is a four-dimensional manifold, whose basis states $|E_{\pm}, S_z = \pm 1/2\rangle$ are characterized by the spin projection $S_z = \pm 1/2$ and by the chirality $C_z = \pm 1$ (which we also label as E_{\pm}). In contrast, antiferromagnetic rings with an even number of spins have non-degenerate $S = 0$ singlet ground state. According to the original proposal in Ref. 16,19, in odd-spin rings the two states of opposite chirality $|E_{\pm}, S_z = M\rangle$ can be coupled linearly by an external electric field, even in the absence of spin-orbit interaction. In order for electric coupling to be non-zero, other criteria must be satisfied.¹⁹ First of all, permanent electric dipoles \mathbf{d}_{ij} must be present on the bridges that mediate the coupling of spin \mathbf{s}_i and \mathbf{s}_j . A necessary (although not sufficient) condition for this is that the superexchange bridge that magnetically couples \mathbf{s}_i and \mathbf{s}_j lacks a center of inversion symmetry. Even when local dipole moments are present on individual bridges, the resulting final spin-electric coupling between chiral states depends in a nontrivial way on the overall symmetry of the molecule. The best way to settle this issue is to carry out a systematic symmetry analysis based on group theory. It

turns out that in triangular spin-1/2 antiferromagnets the coupling is non-zero. On the other hand in pentagon spin 1/2 antiferromagnets, the coupling vanishes, unless spin-orbit interaction is included.¹⁹

We focus now on the spin-electric coupling of chiral states in $\{Cu_3\}$. In the presence of an external electric field $\boldsymbol{\varepsilon}$, The Hamiltonian acquires the additional electric-dipole term $H_{\varepsilon} = \sum_i e\mathbf{r}_i \cdot \boldsymbol{\varepsilon} = e\mathbf{R} \cdot \boldsymbol{\varepsilon}$, where e is the electron charge and \mathbf{r}_i is the coordinate of the i th electron.

In the subspace of spin projection $S_z = 1/2$ of the ground-state manifold, which is invariant for H_{ε} the perturbed Hamiltonian $H_0 + H_{\varepsilon}$ can be expressed in the basis of the chiral states as

$$H = H_0 + H_{\varepsilon} = \begin{vmatrix} \langle E_+, +\frac{1}{2} | H_0 | E_+, +\frac{1}{2} \rangle & \langle E_+, +\frac{1}{2} | H_{\varepsilon} | E_-, +\frac{1}{2} \rangle \\ \langle E_-, +\frac{1}{2} | H_{\varepsilon} | E_+, +\frac{1}{2} \rangle & \langle E_-, +\frac{1}{2} | H_0 | E_-, +\frac{1}{2} \rangle \end{vmatrix}, \quad (7)$$

A similar expression holds for the $S_z = -1/2$ subspace. The eigenvalues of H are

$$E_{\frac{1}{2}}^{\pm}(\boldsymbol{\varepsilon}) = E_{\frac{1}{2}}^{\pm}(0) \pm |\mathbf{d} \cdot \boldsymbol{\varepsilon}|, \quad (8)$$

with $E_{\frac{1}{2}}^{\pm}(0) = \langle E_{\pm}, +\frac{1}{2} | H_0 | E_{\pm}, +\frac{1}{2} \rangle$, and the corresponding eigenstates

$$|\chi_{\frac{1}{2}}^{\pm}(\boldsymbol{\varepsilon})\rangle = \frac{1}{\sqrt{2}} \left(|E_+, +\frac{1}{2}\rangle \pm \frac{|\mathbf{d} \cdot \boldsymbol{\varepsilon}|}{\mathbf{d} \cdot \boldsymbol{\varepsilon}} |E_-, +\frac{1}{2}\rangle \right). \quad (9)$$

Here we have introduced the electric dipole matrix element \mathbf{d} , which couples states of opposite chirality (but with the same spin projection)

$$\mathbf{d} = \langle E_+, +\frac{1}{2} | e\mathbf{R} | E_-, +\frac{1}{2} \rangle. \quad (10)$$

For the specific example of $\{Cu_3\}$ molecule only the matrix elements of X and Y components of \mathbf{R} are nonzero and

$$\langle E_+, +\frac{1}{2} | eX | E_-, +\frac{1}{2} \rangle = i \langle E_+, +\frac{1}{2} | eY | E_-, +\frac{1}{2} \rangle = \frac{d}{\sqrt{2}}, \quad (11)$$

where $d \equiv |\mathbf{d}|$.

The matrix element in Eq. (10) is the key quantity in the spin-electric coupling mechanism. Substituting the expressions for the chiral states from Eqs. (2) and using the orthogonality of spin states we obtain

$$\mathbf{d} = \frac{1}{3} (\langle \Psi_{\downarrow\uparrow\uparrow} | e\mathbf{R} | \Psi_{\downarrow\uparrow\uparrow} \rangle + \omega \langle \Psi_{\uparrow\downarrow\uparrow} | e\mathbf{R} | \Psi_{\uparrow\downarrow\uparrow} \rangle + \omega^2 \langle \Psi_{\uparrow\uparrow\downarrow} | e\mathbf{R} | \Psi_{\uparrow\uparrow\downarrow} \rangle). \quad (12)$$

Evaluating the dipole matrix element between two states of opposite chirality is therefore equivalent to

calculating the dipole moment of each of the three spin configurations. This matrix element determines the strength of spin-electric coupling and we are primarily interested in calculating this quantity by *ab-initio* methods.

Finally, note that all the matrix elements of the electric dipole operator $e\mathbf{R}$ are identically zero in the $S = 3/2$ subspace. This is obvious since $\langle \Psi_{\uparrow\uparrow\uparrow} | e\mathbf{R} | \Psi_{\uparrow\uparrow\uparrow} \rangle$ and $\frac{1}{3}(\langle \Psi_{\downarrow\uparrow\uparrow} | e\mathbf{R} | \Psi_{\downarrow\uparrow\uparrow} \rangle + \langle \Psi_{\uparrow\downarrow\uparrow} | e\mathbf{R} | \Psi_{\uparrow\downarrow\uparrow} \rangle + \langle \Psi_{\uparrow\uparrow\downarrow} | e\mathbf{R} | \Psi_{\uparrow\uparrow\downarrow} \rangle)$ are both zero by symmetry. We will confirm this result by direct *ab-initio* calculations.

B. Effective spin Hamiltonian description

The effect of the electric field on the the low-energy spectrum of $\{Cu_3\}$ can be recast in the form of the effective spin model introduced in Sec. II B. Since the electric dipole operator has nonzero matrix elements only in the ground-state manifold, where it couples states with equal spin components and opposite chirality, we expect that the spin-electric Hamiltonian H_ε can be rewritten as a linear combination of the ladder operators C_\pm . By comparing the matrix elements of H_ε given in Eq. (10) and (11) with the action of C_\pm on the chiral states, one can show that¹⁹

$$H_\varepsilon^{\text{eff}} = \frac{d}{\sqrt{2}} \boldsymbol{\varepsilon}' \cdot \mathbf{C}_\parallel, \quad (13)$$

where $\boldsymbol{\varepsilon}' = R_z(\phi)(7\pi/6 - 2\theta)\boldsymbol{\varepsilon}$, with $R(\phi)$ being the matrix representing a rotation by an angle ϕ around the z -axis, and θ being the angle between the in-plane component $\boldsymbol{\varepsilon}_\parallel$ of the electric field and the bond $\mathbf{s}_1 - \mathbf{s}_2$. By using Eq. (5) and (6) we can now rewrite $\mathbf{C}_\parallel = (C_x, C_y)$ in term of spin-operators \mathbf{s}_i and we obtain¹⁹

$$H_\varepsilon^{\text{eff}} = \sum_i^3 \delta J_{ii+1}(\boldsymbol{\varepsilon}) \mathbf{s}_i \cdot \mathbf{s}_j, \quad (14)$$

where the modified exchange parameters take the form¹⁹

$$\delta J_{ii+1}(\boldsymbol{\varepsilon}) = \frac{4d}{3\sqrt{2}} |\boldsymbol{\varepsilon}_\parallel| \cos\left(\frac{2\pi}{3}i + \theta\right). \quad (15)$$

This expression of the effective electric-dipole Hamiltonian suggests a transparent physical interpretation of the spin-electric coupling mechanism.^{16,19} An external electric field changes the charge distribution of the $\{Cu_3\}$ molecule which, in turn, changes the exchange interaction between neighboring atoms. Since the modified exchange interaction does not commute with H_0 , it can cause

transitions between chiral states within the ground-state manifold.

In Eq. (15), $\boldsymbol{\varepsilon}_\parallel$ is the projection of electric field on the Cu_3 plane (in our case $\boldsymbol{\varepsilon}_\parallel = \boldsymbol{\varepsilon}$), $i=1$ and $\theta = 30^\circ$ is the angle between $\boldsymbol{\varepsilon}$ and the line joining Cu_1 and Cu_2 . Finally, note that Eqs. (14) and (15) provide an estimate of the dependence of the ground-state energy as function of the electric field. Since in the absence of spin-orbit coupling the electric-dipole Hamiltonian has zero matrix elements in the $S = 3/2$ subspace, Eq. (15) gives us an estimate of the dependence of the exchange constant J (proportional to the splitting between the $S = 1/2$ ground state and $S = 3/2$ excited state) on $\boldsymbol{\varepsilon}$.

IV. AB-INITIO EVALUATION OF THE SPIN-ELECTRIC COUPLING

A. Calculation of the electric dipole moment

To construct the chiral states of the full $\{Cu_3\}$ molecule, we have calculated the ground state of the molecule for different spin configurations, as shown in Fig. 4. Although there are two doublets of chiral states for the triangular arrangement of three spin $1/2$ atoms, in this calculation we have used only one doublet associated with the spin projection $+1/2$, since we are interested in coupling between states of opposite chirality with the same spin projection.

To study the spin-electric effect we have applied an external field along the perpendicular bisectors between positions 2 and 3 of the Cu_3 triangle shown in Fig. 5, and have calculated the corresponding ground state energy self-consistently for different spin configurations. We have kept the direction of the field relative to coordinate axes fixed, and have changed the orientation of the spins at the Cu atoms to generate the three possible spin configurations of the $\{Cu_3\}$ molecule.

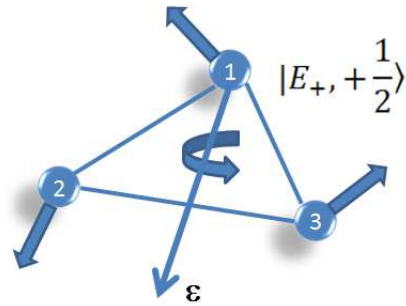


FIG. 5: The direction of the applied electric fields used in this calculation.

Our calculations show that $\{Cu_3\}$ molecule in the spin $S_z = 3/2$ state does not have any permanent electric-dipole moment. On the other hand each of the three frustrated spin $S_z = 1/2$ configurations have a small permanent (i.e, zero-field) dipole moment, as expected from the general discussion of Sec. III. The three moments have all the same magnitude but their directions are along the perpendicular bisector of Cu_3 triangle and between two Cu atoms with parallel spin alignments. The relative orientations of these moments along with components are shown in Fig. 6. The fact that the $S_z = 3/2$ state does not have permanent dipole moment whereas $S_z = 1/2$ states do, suggests that the dipole moments are solely due to spin effects.

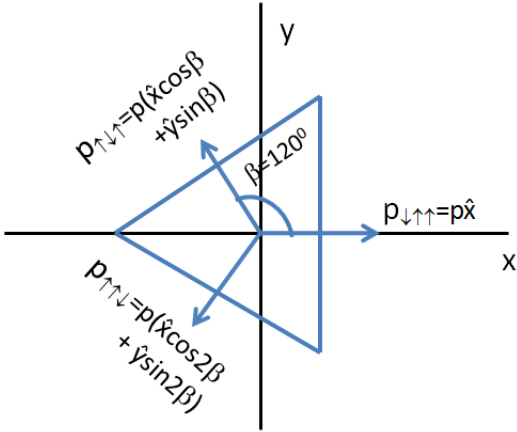


FIG. 6: Dipole moments of three spin configurations and their relative angles. $\mathbf{p}_{\downarrow\uparrow\uparrow} = \langle \Psi_{\downarrow\uparrow\uparrow} | e\mathbf{R} | \Psi_{\downarrow\uparrow\uparrow} \rangle$, $\mathbf{p}_{\uparrow\uparrow\uparrow} = \langle \Psi_{\uparrow\uparrow\uparrow} | e\mathbf{R} | \Psi_{\uparrow\uparrow\uparrow} \rangle$ and $\mathbf{p}_{\uparrow\uparrow\downarrow} = \langle \Psi_{\uparrow\uparrow\downarrow} | e\mathbf{R} | \Psi_{\uparrow\uparrow\downarrow} \rangle$ are the moments corresponding to the spin configurations of Fig. 4a.

In the presence of an electric field the energies of the $\{Cu_3\}$ molecule are slightly lower when field is between two Cu atoms with parallel spins than for the other two spin configurations, where the field is between two Cu atoms with anti-parallel spin alignments. This difference in energy is due to the direction of permanent moment relative to the induced moment. We have calculated the permanent dipole-moment of the ground state spin configuration by fitting the dependence of energy of one of the $S_z = 1/2$ spin configurations with external field, as shown in Fig. 7. The calculated values of the permanent dipole moment and polarizability of $\{Cu_3\}$ molecule are $p = 4.77 \times 10^{-33} C.m$ and $\alpha = 1.025 \times 10^{-38} C.m^2/V$, respectively. Although there is no experimental value of polarizability available for $\{Cu_3\}$, polarizabilities within DFT calculations are generally accurate to 1-3 percent.

The value p extracted from this fitting is consis-

tent with the direct calculation of the electric dipole moment of the three spin configurations at zero field, implemented in the NRLMOL.

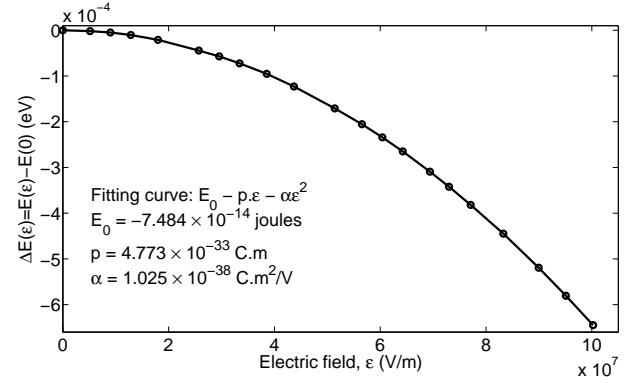


FIG. 7: Electric field dependence of the energy for one of the three spin $S_z = 1/2$ spin configurations. The plot for the other two configurations is very similar and the fitting yields essentially the same values of p and α .

To calculate the matrix element \mathbf{d} given in Eq. (12), we substitute the components of the moments for the different spin configurations of Fig. 6,

$$\begin{aligned} \mathbf{d} &= \frac{1}{3}p[(1 + \omega \cos \beta + \omega^2 \cos 2\beta)\hat{\mathbf{x}} \\ &\quad + (\omega \sin \beta + \omega^2 \sin 2\beta)\hat{\mathbf{y}}] \\ &= \frac{p}{2}(\hat{\mathbf{x}} + i\hat{\mathbf{y}}). \end{aligned} \quad (16)$$

The magnitude of the dipole coupling in $\{Cu_3\}$ molecule is, therefore

$$d = \frac{p}{\sqrt{2}} = 3.38 \times 10^{-33} C.m. \quad (17)$$

The efficiency of the $\{Cu_3\}$ molecule as a switching device depends on how fast an electric field can generate transitions from one chiral state to the other. The characteristic (Rabi) time for transitions between the two chiral states is given by

$$\tau = \frac{h}{|\mathbf{d} \cdot \boldsymbol{\epsilon}|}. \quad (18)$$

Here, h is Planck constant, \mathbf{d} is the dipole matrix element between states of different chirality given by Eq. (17), and $\boldsymbol{\epsilon}$ is the external electric field. Fig. 8 shows the dependence of the Rabi time on external field, with the maximum value of ≈ 50 ns for a field $\epsilon \simeq 5 \times 10^6$ V/m. For larger fields of the order of $\simeq 10^8$ V/m, easily attainable in the vicinity of a STM tip, the Rabi time is of the order of 1 ns, which is considered to be a relatively fast control-time in quantum information processing.

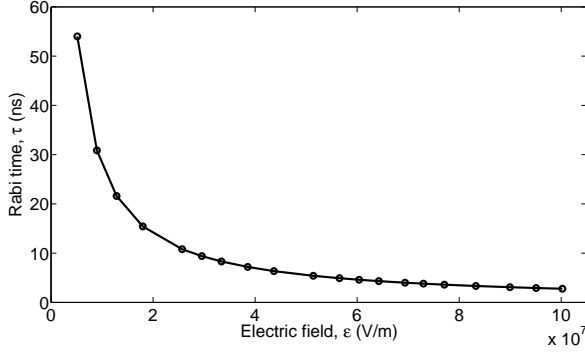


FIG. 8: Electric field dependence of the Rabi time for quantum transitions between the two (ground-state).

B. Modification of the exchange coupling in an electric field

To calculate the dependence of the exchange coupling J on the electric field, we need to determine how the spin $S = 1/2$ ground state and the spin $S = 3/2$ excited state depend on the field. We define the exchange energy $J(\boldsymbol{\epsilon})$ as the difference

$$J(\boldsymbol{\epsilon}) = E_{\frac{3}{2}}(\boldsymbol{\epsilon}) - E_{\frac{1}{2}}^-(\boldsymbol{\epsilon}), \quad (19)$$

where $E_{\frac{1}{2}}(\boldsymbol{\epsilon})$ and $E_{\frac{3}{2}}(\boldsymbol{\epsilon})$ are the energies of the $S = 1/2$ ground-state and of the spin $S = 3/2$ excited state respectively in the presence of an electric field.

Based on our discussion of Sec. III.A [see Eq. (8)], the energy of the $S = 1/2$ chiral ground-state manifold and the $S = 3/2$ excited state vs $\boldsymbol{\epsilon}$ are shown schematically in Fig. 9, where we have disregarded the quadratic dependence of both $E_{\frac{3}{2}}$ and $E_{\frac{1}{2}}$ on the field due to the induced electric dipole moment.

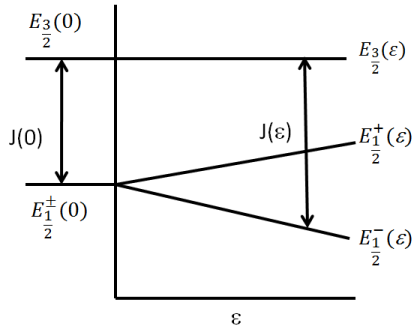


FIG. 9: Schematic electric-field dependence of the energies of the $S = 1/2$ chiral states and spin $S = 3/2$ excited state, and the exchange energy J defined in Eq. (19).

The calculation of the electric-field-modified exchange parameter using first-principle methods is

not completely straightforward, since the SDFT calculations done within NRLMOL allow us to calculate the energy of a given spin configuration, whereas the (chiral) ground-state is a linear combination of three possible spin configurations. However, we can get an estimate of the dependence of J on $\boldsymbol{\epsilon}$ by approximating

$$\begin{aligned} E_{\frac{1}{2}}^-(\boldsymbol{\epsilon}) &\approx \alpha_1^2 \langle \Psi_{\downarrow\uparrow\uparrow} | H_{DFT}(\boldsymbol{\epsilon}) | \Psi_{\downarrow\uparrow\uparrow} \rangle \\ &\quad + \alpha_2^2 \langle \Psi_{\uparrow\downarrow\uparrow} | H_{DFT}(\boldsymbol{\epsilon}) | \Psi_{\uparrow\downarrow\uparrow} \rangle \\ &\quad + \alpha_3^2 \langle \Psi_{\uparrow\uparrow\downarrow} | H_{DFT}(\boldsymbol{\epsilon}) | \Psi_{\uparrow\uparrow\downarrow} \rangle \\ &= \alpha_1^2 E_{\downarrow\uparrow\uparrow} + \alpha_2^2 E_{\uparrow\downarrow\uparrow} + \alpha_3^2 E_{\uparrow\uparrow\downarrow}. \end{aligned}$$

The coefficients α 's can be obtained by expanding $|\chi_{\frac{1}{2}}^-(\boldsymbol{\epsilon})\rangle$ in Eq. (9) in terms of the spin configurations, which leads to

$$\begin{aligned} |\chi_{\frac{1}{2}}^-(\boldsymbol{\epsilon})\rangle &= \frac{1}{\sqrt{6}} [(1-r)\Psi_{\downarrow\uparrow\uparrow} + (\omega - \omega^2 r)\Psi_{\uparrow\downarrow\uparrow} \\ &\quad + (\omega^2 - \omega r)\Psi_{\uparrow\uparrow\downarrow}] \\ &= \alpha_1 \Psi_{\downarrow\uparrow\uparrow} + \alpha_2 \Psi_{\uparrow\downarrow\uparrow} + \alpha_3 \Psi_{\uparrow\uparrow\downarrow}, \quad (20) \end{aligned}$$

where $r = \frac{|\mathbf{d}\cdot\boldsymbol{\epsilon}|}{\mathbf{d}\cdot\boldsymbol{\epsilon}} = \frac{1}{\sqrt{2}}(1-i)$, for the given choice of the electric field direction.

Therefore,

$$\begin{aligned} E_{\frac{1}{2}}^-(\boldsymbol{\epsilon}) &\approx \frac{1}{6} \left[(2 - \sqrt{2}) E_{\downarrow\uparrow\uparrow} + \left(2 + \frac{1 - \sqrt{3}}{\sqrt{2}} \right) E_{\uparrow\downarrow\uparrow} \right. \\ &\quad \left. + \left(2 + \frac{1 + \sqrt{3}}{\sqrt{2}} \right) E_{\uparrow\uparrow\downarrow} \right]. \quad (21) \end{aligned}$$

The energies $E_{\uparrow\downarrow\uparrow}$ and $E_{\uparrow\uparrow\downarrow}$ are the same because of symmetry. Since the difference between $E_{\downarrow\uparrow\uparrow}$ and $E_{\uparrow\downarrow\uparrow}$ is very small and near the accuracy limit of our calculations, we further approximate $E_{\downarrow\uparrow\uparrow} \approx E_{\uparrow\downarrow\uparrow}$.

The exchange parameter J becomes

$$J(\boldsymbol{\epsilon}) \approx E_{\uparrow\uparrow\uparrow}(\boldsymbol{\epsilon}) - E_{\downarrow\uparrow\uparrow}(\boldsymbol{\epsilon}), \quad (22)$$

with $E_{\uparrow\uparrow\uparrow}(\boldsymbol{\epsilon}) \equiv E_{\frac{3}{2}}(\boldsymbol{\epsilon})$.

In Fig. 10 we plot the electric-field-induced variation of the exchange energy $\delta J(\boldsymbol{\epsilon}) \equiv J(\boldsymbol{\epsilon}) - J(0)$ vs. $\boldsymbol{\epsilon}$. The result for δJ obtained by evaluating Eq. (22) with SDFT is shown by the red curve. For this part of the calculations the convergence criterion has been increased up to 10^{-8} Hartree. We can see that the dependence of J on electric field is quite small, and δJ is in the μeV range for electric fields $\boldsymbol{\epsilon} = (1 - 10) \times 10^7$ V/m. These energies are not far from the accuracy limit of our numerical calculations, which is the reason of the fluctuations seen in the plot. Nevertheless the overall trend is

an increase of $\delta J(\varepsilon)$ with ε , which is approximately linear at low fields. Note that the SDFT evaluations of $E_{\uparrow\uparrow\uparrow}(\varepsilon)$ and $E_{\downarrow\uparrow\uparrow}(\varepsilon)$ contain a quadratic contribution in ε but this nearly cancels at small fields when computing δJ , and it becomes appreciable only at $\varepsilon \geq 5 \times 10^7$ V/m.

The blue line in Fig. 10 shows the dependence of δJ on ε given by the prefactor of the cosine function in Eq. (15), which was derived within the spin Hamiltonian formalism. When plotting Eq. (15) we have used the value of d extracted from our first-principle calculations. Comparing the two curves, we note that, apart from the fluctuations in the numerical result mentioned above, the theoretical and numerical values for δJ are consistent, and both procedures predict an overall increase of δJ with electric field.

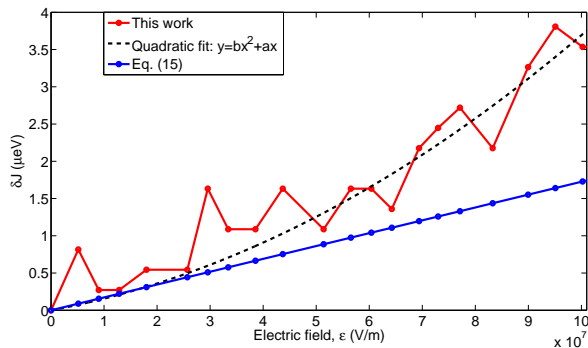


FIG. 10: Electric-field dependence of the variation of the exchange energy $\delta J(\varepsilon) \equiv J(\varepsilon) - J(0)$ induced by the field. The red curve is the first-principle result obtained by evaluating Eq. (22) and the dashed black curve is the quadratic fit of $\delta J(\varepsilon)$. The blue curve is a plot of Eq. (15) with the numerical value of d extracted from the first-principle calculations.

V. SUMMARY

In this paper we have carried out a first-principle study of the spin-electric coupling in single-molecule magnets (SMMs) without inversion symmetry. Specifically, we have analyzed the clear-cut case of the $\{Cu_3\}$ triangular antiferromagnet where, because of spin frustration, the ground-state consists of two generate spin 1/2 doublets of opposite chirality. Theory predicts^{16,19} that an electric field can couple these states, even when spin-orbit interaction is absent. The main goal of our work has been to compute how strong this coupling is.

Our calculations of the electronic structure of the $\{Cu_3\}$ molecule show that the spin magnetic mo-

ments are localized at the three Cu atom sites of the molecule. The magnetic properties of the molecule are correctly described by a triangular spin $s = 1/2$ Heisenberg antiferromagnet, with an exchange coupling J of the order of 5 meV that separates the energies of the spin- $S = 1/2$ ground-state manifold and the spin- $S = 3/2$ excited states. In agreement with theoretical predictions,^{16,19} we find that an electric field couples the two ground-state doublets of opposite chirality, even when spin-orbit interaction is absent. The strength of the coupling is linear in the field and proportional to the permanent electric dipole moment d of the three frustrated spin configurations. The calculations yield a value of $d \approx 4 \times 10^{-33}$ C m $\approx e10^{-4}a$ for $\{Cu_3\}$, where a is the Cu atom separation. Corresponding Rabi times for electric-field-induced transitions between chiral states can be as short as 1 ns, for electric fields of the order of 10^8 V/m, which are easily produced by a nearby STM tip. Thus this spin-electric coupling mechanism is of potential interest for the use of single-molecule magnets in quantum information processing as fast switching devices.

Our calculations also indicate that the presence of an external electric field modifies the exchange constant J . Typically the electric field increases J , although the energy scale of this change is in the μeV range for typical STM-generated electric fields. Thus for this specific antiferromagnetic SMM, the electric field cannot trigger directly a level crossing between magnetic states with different total spin, as suggested recently for other SMMs.^{30,31}

This work shows that a microscopic investigation of the spin-electric coupling using the NRL-MOL first-principle code is feasible, and can systematically implemented for a large class of SMMs which lack inversion symmetry. In this paper we have disregarded the effect of spin-orbit interaction and external magnetic field. The spin-orbit interaction strength is small compared to the exchange coupling J . In the case of $\{Cu_3\}$ it simply introduces a small splitting between the chiral states, but is not expected to influence significantly the spin-electric coupling. However in other antiferromagnetic rings with an odd number of spins spin-orbit interaction is essential for the very existence of the coupling mechanism.¹⁹ Work to include both spin-orbit interactions and an external magnetic field is in progress. Together with the group-theory analysis presented in Ref. 19, these studies will be a considerable help in guiding future experiments and selecting the most promising SMMs for applications in quantum information processing and nanospintronics.

Acknowledgment

We would like to thank Daniel Loss for introducing us to this problem and for several useful dis-

cussions. This work was supported by the Faculty of Natural Sciences at Linnaeus University, and the Swedish Research Council under Grant No: 621-2007-5019.

-
- ¹ D. Gatteschi, R. Sessoli, and J. Villain, *Molecular Nanomagnets* (Oxford University Press, Oxford, 2006).
 - ² J. R. Friedman, M. P. Sarachik, J. Tejada, and R. Ziolo, *Phys. Rev. Lett.* **76**, 3830 (1996).
 - ³ L. Thomas, F. Lionti, R. Ballou, D. Gatteschi, R. Sessoli, and B. Barbara, *Nature* **383**, 145 (1996).
 - ⁴ W. Wernsdorfer and R. Sessoli, *Science* **284**, 133 (1999).
 - ⁵ A. Ardavan, O. Rival, J. J. L. Morton, S. J. Blundell, A. M. Tyryshkin, G. A. Timco, and R. E. P. Winpenny, *Phys. Rev. Lett.* **98**, 057201 (2007).
 - ⁶ A. R. Rocha, V. M. Garcia-Suarez, S. W. Bailey, C. J. Lambert, J. Ferrer, and S. Sanvito, *Nat. Mater.* **4**, 335 (2005).
 - ⁷ S. Sanvito and A. R. Rocha, *Journal of Computational and Theoretical Nanoscience* **3**, 624 (2006).
 - ⁸ A. R. Rocha, V. M. Garcia-Suarez, S. Bailey, C. Lambert, J. Ferrer, and S. Sanvito, *Phys. Rev. B* **73**, 085414 (2006).
 - ⁹ M. H. Jo, J. E. Grose, K. Baheti, M. M. Deshmukh, J. J. Sokol, E. M. Rumberger, D. N. Hendrickson, J. R. Long, H. Park, and D. C. Ralph, *Nano Lett.* **6**, 2014 (2006).
 - ¹⁰ H. B. Heersche, Z. de Groot, J. A. Folk, H. S. J. van der Zant, C. Romeike, M. R. Wegewijs, L. Zobbi, D. Barreca, E. Tondello, and A. Cornia, *Phys. Rev. Lett.* **96**, 206801 (2006).
 - ¹¹ L. Bogani and W. Wernsdorfer, *Nat. Mater.* **7**, 179 (2008).
 - ¹² M. N. Leuenberger and D. Loss, *Nature* **410**, 789 (2001).
 - ¹³ J. Lehmann, A. Gaita-Arino, E. Coronado, and D. Loss, *Nat Nano* **2**, 312 (2007).
 - ¹⁴ C. F. Hirjibehedin, C. P. Lutz, and A. J. Heinrich, *Science* **312**, 1021 (2006).
 - ¹⁵ A. C. Bleszynski-Jayich, L. E. Frberg, M. T. Bjrk, H. J. Trodahl, L. Samuelson, and R. M. Westervelt, *Phys. Rev. B* **77**, 245327 (2008).
 - ¹⁶ M. Trif, F. Troiani, D. Stepanenko, and D. Loss, *Phys. Rev. Lett.* **101**, 217201 (2008).
 - ¹⁷ U. Kortz, N. K. Al-Kassem, M. G. Savelieff, N. A. Al Kadi, and M. Sadakane, *Inorg. Chem.* **40**, 4742 (2001).
 - ¹⁸ K.-Y. Choi, Y. H. Matsuda, H. Nojiri, U. Kortz, F. Hussain, A. C. Stowe, C. Ramsey, and N. S. Dalal, *Phys. Rev. Lett.* **96**, 107202 (2006).
 - ¹⁹ M. Trif, F. Troiani, D. Stepanenko, and D. Loss, *Phys. Rev. B* **82**, 045429 (2010).
 - ²⁰ M. R. Pederson and S. N. Khanna, *Phys. Rev. B* **60**, 9566 (1999).
 - ²¹ M. Pederson, D. Porezag, J. Kortus, and D. Patton, *physica status solidi (b)* **217**, 197 (2000).
 - ²² J. Kortus, M. R. Pederson, T. Baruah, N. Bernstein, and C. S. Hellberg, *Polyhedron* **22**, 1871 (2003).
 - ²³ A. V. Postnikov, J. Kortus, and M. R. Pederson, Newsletter 61 of the ψ_k -Network (2004), URL http://psi-k.dl.ac.uk/newsletters/News_61/Highlight_61.pdf.
 - ²⁴ L. Michalak, C. M. Canali, M. R. Pederson, M. Paulsson, and V. G. Benza, *Phys. Rev. Lett.* **104**, 073004 (2010).
 - ²⁵ A. Kokalj, *J. Mol. Graphics Modeling* **17**, 176 (1999), URL <http://www.xcrysden.org>.
 - ²⁶ M. R. Pederson and K. A. Jackson, *Phys. Rev. B* **41**, 7453 (1990).
 - ²⁷ K. Jackson and M. R. Pederson, *Phys. Rev. B* **42**, 3276 (1990).
 - ²⁸ J. P. Perdew, K. Burke, and M. Ernzerhof, *Phys. Rev. Lett.* **77**, 3865 (1996).
 - ²⁹ A. Stowe, S. Nellutla, N. Dalal, and U. Kortz, *Eur. J. Inorg. Chem.* **2004**, 3792 (2004).
 - ³⁰ N. Baadji, M. Piacenza, T. Tugsuz, F. D. Sala, G. Maruccio, and S. Sanvito, *Nat. Mat.* **8**, 813 (2009).
 - ³¹ E. A. Osorio, K. Moth-Poulsen, H. S. J. van der Zant, J. Paaske, P. Hedegård, K. F. J. Bendix, and T. Bjørnholm, *Nanolett.* **10**, 105 (2010).